

Generation of vortex dipoles in superfluid Fermi gas in BCS limit

S. Gautam¹

¹*Physical Research Laboratory, Navarangpura, Ahmedabad - 380 009, India*

(Dated: April 10, 2019)

We theoretically investigate the generation of the vortex dipoles in superfluid Fermi gas in the BCS limit. The vortex dipoles are generated in superfluid either by moving an obstacle above a critical speed or due to the decay of the shock waves obtained on the sudden mixing of two superfluid fragments. We observe that in pancake-shaped traps, the shock waves can lead to the formation of density ripples, which decay into vortex dipoles due to the onset of snake instability.

PACS numbers: 03.75.Ss, 03.75.Kk, 03.75.Lm

I. INTRODUCTION

One of the unique feature of the superfluids is that these can support only quantized vortices. In this context, the experimental observation of the vortex lattice across the Bardeen-Cooper-Schrieffer to Bose-Einstein condensate (BCS-BEC) cross-over has unequivocally proved the superfluid nature of these systems [1]. In the experiment, vortices were created by rotating the trapped superfluid Fermi gas using a blue detuned laser beam. In a recent experiment [2] with pancake-shaped BEC, a pair of vortices with opposite circulation were generated by moving an obstacle potential above a critical speed, which is equal to the fraction of the local sound speed. This vortex-antivortex pair is nothing but two dimensional analogue of vortex rings. In Bose-Einstein condensates (BECs), vortex rings have been experimentally generated from the dark solitons, which undergo long wavelength transverse instability called snake instability [3]. Vortices and vortex dipoles can also be generated by merging and interfering of multiple trapped BECs [4]. The decay of shock waves into vortex dipoles has also been observed in BECs [5]. The decay is mediated by the formation of solitons which decay via snake instability. In the non-linear Kerr-like medium, the propagation, non-linear response, and collisions between the dispersive superfluid-like shock waves have been experimentally observed [6]. Shock waves have also been generated by merging or splitting BECs non-adiabatically [7]. The same method has been used to generate the shock waves in superfluid Fermi gas at unitarity [8]. Unlike BECs, the soliton mediated decay of shock waves into vortex dipoles has not been unambiguously detected in superfluid Fermi gases. In a recent work [9], formation of shock waves and domain walls in strongly interacting Fermi superfluid has been investigated theoretically, and the possibility of snake instability was conjectured in sufficiently wide traps. The formation and dynamics of sub- and supersonic shock waves, using zero temperature equations of generalized superfluid hydrodynamics, have also been studied in unitary Fermi gas [10].

Although vortex dipoles and vortex rings are yet to be experimentally realized in superfluid Fermi gases, it is well established that vortex antivortex pairs play very im-

portant roles in superfluid turbulence [11] and Berezinskii Kosterlitz Thouless (BKT) phase transition [12, 13]. Recently using local extension of the time-dependent density functional theory, real time dynamics of quantized vortex rings in unitary Fermi gas in cylindrical traps was theoretically investigated in Ref. [14].

The advent of ultracold fermions in optical lattices [15], which are almost pure realization of Hubbard model [16], has lead to the flurry of research investigations. These systems are now routinely used, both by experimentalists and theorists, to understand the strongly correlated systems. In this context, Mott insulator of fermionic atoms in an optical lattice has already been experimentally realized [17, 18]. On the theoretical front, dynamical mean field theory (DMFT) [19] has been successfully used to study these strongly correlated systems in three dimensions [20, 21]. The DMFT neglects the non-local correlations, which can no longer be done in lower dimensions and frustrated systems. For these systems, cluster extension of DMFT like dynamical cluster approximation (DCA) and cellular dynamical mean-field theory (CDMFT) have been used to study these systems [22–24]. A key recent development in the field, has been the experimental realization of spin-orbit coupling (SOC) [25, 26]. The interplay between SOC and interatomic interactions leads to many interesting phenomena [27]. Recently, finite temperature phase diagram of two-component atomic Fermi gas with population imbalance in the presence of Rashba spin orbit coupling has been studied in Ref. [28].

In the present work, we numerically study the generation of vortex dipoles in an oblate superfluid Fermi gas (SFG) in BCS limit. We employ two methods, namely (a) vortex dipole generation by a moving obstacle and (b) soliton mediated decay of shock waves, to this end. At $T = 0K$, when the normal component in the superfluid tends to zero, a theoretical approach based on the Gallilei-invariant density functional theory has been developed in Refs. [29–37] to study the superfluid Fermi gases. This theoretical approach allows one to write a non-linear Schrödinger equation (NLSE) for the BCS superfluid that leads to the same superfluid density as the original many body fermion system [30]. For the applicability of this NLSE for the BCS superfluid, the character-

istic wavelength of the phenomenon under study must be larger than the healing length. The NLSE has been used to study the collective excitations [30, 32], free expansion of the superfluid Fermi gas [33], superfluid-insulator transition [38], and solitons [35, 36].

The paper is organized as follows. In Sec. II we study the evolution of the BCS superfluid with a repulsive obstacle moving across it. In Sec. III we study the generation of the shock wave by non-adiabatically merging two superfluid fragments followed by the decay of shock waves into vortex dipoles. This is followed by conclusions in Sec. IV.

II. GENERATION OF THE VORTEX DIPOLES BY THE REPULSIVE POTENTIALS

Barring normalization factors, the order parameter for the superfluid bosonic and fermionic systems are

$$\begin{aligned}\Xi_B(\mathbf{r}, t) &= \langle \hat{\psi}(\mathbf{r}, t) \rangle, \\ \Xi_F(\mathbf{r}, t) &= \langle \hat{\psi}_\downarrow(\mathbf{r}, t) \hat{\psi}_\uparrow(\mathbf{r}, t) \rangle,\end{aligned}\quad (1)$$

respectively, where $\psi(\mathbf{r}, t)$ and $\psi_\sigma(\mathbf{r}, t)$ with $\sigma = \uparrow$ or \downarrow are the bosonic and fermionic annihilation field operators, respectively. In case of bosons, the order parameter is the wavefunction of the macroscopically occupied single particle state. Similarly, the order parameter can be considered as the wavefunction of the macroscopically occupied two particle state for Fermi superfluids. The order parameter is normalized to total number of condensed bosons [39] or condensed Cooper pairs [40–43]. In the BCS limit, the s -wave scattering length between two hyperfine states of the Fermi gas $a \rightarrow -0$. In this limit, the superfluid Fermi gas, consisting of equal number of two components, at $T = 0$ K is described by mean field equation [29–37]

$$\begin{aligned}\left[-\frac{\hbar^2}{4m} \nabla^2 + \frac{2\hbar^2}{m_p} (3\pi^2)^{2/3} |\psi(\mathbf{r}, t)|^{4/3} + V(\mathbf{r}, t) \right] \psi(\mathbf{r}, t) \\ = i\hbar \frac{\partial \psi(\mathbf{r}, t)}{\partial t},\end{aligned}\quad (2)$$

where $\psi(\mathbf{r}, t)$ is complex order parameter for the SFG, m is the atomic mass of the fermionic species, $m_p = 2m$ is the mass of the fermionic pair, and $V(\mathbf{r})$ is the trapping potential. In the aforementioned equation, $\psi(\mathbf{r}, t)$ is normalized to the number of fermions N , i.e., $\int |\psi(\mathbf{r}, t)|^2 d\mathbf{r} = N$; this normalization is different from the normalization of the $\Xi_F(\mathbf{r}, t)$ [39, 42, 43]. In terms of $\psi(\mathbf{r}, t)$ the energy of the SFG is [29, 34]

$$E = \int \left[\frac{\hbar^2}{4m} |\nabla \psi|^2 + \frac{3\hbar^2}{5m} (3\pi^2)^{2/3} |\psi|^{10/3} + V(\mathbf{r}, t) |\psi|^2 \right] d\mathbf{r},$$

here $\psi = \psi(\mathbf{r}, t)$. In the present work, we consider pancake-shaped trapping potential

$$V(\mathbf{r}, t) = \frac{m_p \omega^2}{2} (x^2 + y^2 + \alpha^2 z^2) + V_{\text{obs}}(\mathbf{r}, t), \quad (3)$$

where ω is the radial trapping frequency, $\alpha \gg 1$ is the ratio of axial to radial trapping frequency, and V_{obs} is the obstacle potential which can be attractive or repulsive. We consider SFG of ^{40}K with $N = 10^3$, $\omega = 10\text{Hz}$, $\alpha = 10$, and

$$V_{\text{obs}}(\mathbf{r}, t) = V_0 \exp \left\{ -2 \frac{[(x - x_0(t))^2 + (y - y_0(t))^2]}{w_0^2} \right\},$$

here $(x_0(t), y_0(t), 0)$ is the instantaneous location of the Gaussian obstacle potential with $1/e^2$ width equal to w_0 . In Ref. [44], effective two dimensional (2D) equations for the pancake-shaped Fermi superfluids in both the BCS and unitary limit ($a \rightarrow -\infty$) have been proposed. These 2D equations provide a good approximation to the real three dimensional (3D) systems. In the present work, instead of using these 2D equations, we consider the full three dimensional equation and solve it numerically using the split time step Crank-Nicolson method [45]. We can rewrite the Eq. 2 in scaled units using the transformations

$$\begin{aligned}\mathbf{r} &= \mathbf{r}' a_{\text{osc}}, \quad t = t' \omega^{-1}, \\ \psi(\mathbf{r}, t) &= \frac{\sqrt{N} \phi(\mathbf{r}', t')}{a_{\text{osc}}^{3/2}},\end{aligned}\quad (4)$$

where the primed quantities are in scaled units and $a_{\text{osc}} = \sqrt{\hbar/(m_p \omega)}$ is the oscillator length. After dropping the primes, the scaled NLSE describing the superfluid Fermi gas in BCS limit is

$$\begin{aligned}\left[-\frac{\nabla^2}{2} + 2(3\pi^2 N)^{2/3} |\phi|^{4/3} + V(\mathbf{r}, t) \right] \phi(\mathbf{r}, t) \\ = i \frac{\partial \phi(\mathbf{r}, t)}{\partial t},\end{aligned}\quad (5)$$

We consider the repulsive Gaussian obstacle potentials with $V_0 = 93\hbar\omega$, $x_0 = -6a_{\text{osc}}$, $w_0(0) = 10.0\mu\text{m}$ and move it along x -axis. While moving the obstacle we continuously decrease the strength of obstacle potential such that it vanishes at $x_0 = 6a_{\text{osc}}$. As is expected, we find that there is no generation of the vortices if the obstacle is moved below the critical speed. For example, Fig. 1 shows the evolution of the superfluid density when the obstacle is moved with the sub-critical speed of $150\mu\text{m/s}$. On the other hand, when the obstacle is moved with a speed greater than the critical speed, vortex dipoles are produced. The generation of a vortex dipole for the obstacle potential moving with a super-critical speed of $175\mu\text{m/s}$ is shown in Fig. 2. The critical speed for vortex nucleation is a fraction of the speed of the local speed of sound. In case homogeneous BCS superfluid, the speed

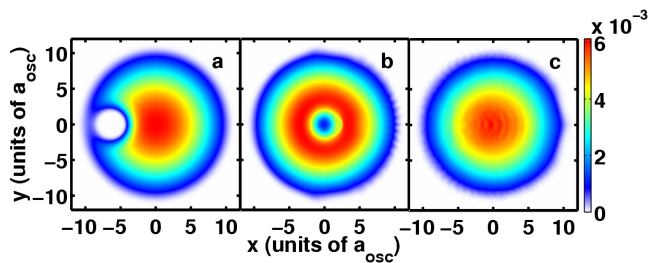


FIG. 1: (Color online) Evolution of the superfluid Fermi gas in BCS limit when the obstacle is moving with the sub-critical speed of $150 \mu\text{m/s}$. Images with labels (a), (b), (c) are the superfluid densities $|\phi(\mathbf{r}, t)|^2$ in units of a_{osc}^{-3} on xy plane at $t = 0$ ms, $t = 143$ ms, and $t = 286$ ms respectively.

of the sound [46] $c = v_F/\sqrt{3}$, where $v_F = 2(3\pi^2 N|\psi|^2)^{1/3}$ (in scaled units) is the Fermi velocity. For the parameters considered in the present work, the maximum speed of sound at the trap center is $\sim 1465 \mu\text{m/s}$. This is only an approximate value since the presence of the trapping potential changes the speed of the sound from its value for homogeneous case [47]. When the obstacle moves across

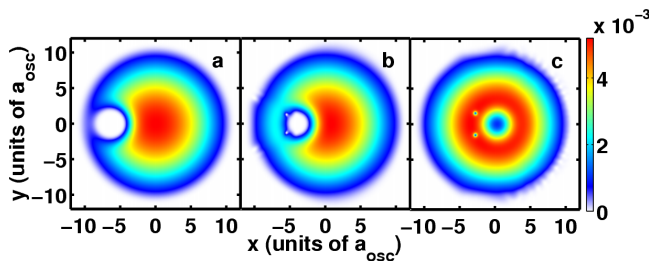


FIG. 2: (Color online) Evolution of the superfluid Fermi gas in BCS limit when the obstacle is moving with the supercritical speed of $175 \mu\text{m/s}$. Images with labels (a), (b), and (c) show the superfluid densities $|\phi(\mathbf{r}, t)|^2$ in units of a_{osc}^{-3} on xy plane at $t = 0$ ms, $t = 48$ ms, and $t = 127$ ms respectively.

the superfluid with the sub-critical speed, it can still generate sound waves. The generation of the sound waves can be inferred from the variation of superfluid kinetic energy with time. The total kinetic energy KE of the superfluid in scaled units is

$$\begin{aligned} KE &= \int \frac{(\nabla|\phi|)^2}{2} d\mathbf{r} + \int \frac{(|\phi|\nabla\theta)^2}{2} d\mathbf{r}, \\ &= KE_q + KE_s \end{aligned} \quad (6)$$

where θ is the phase of superfluid wavefunction ϕ . The first energy term KE_q is the quantum pressure energy and the second KE_s is the energy arising from the superfluid velocity. After the obstacle potential has become zero, the total energy almost becomes constant as is shown in Fig. 3(a). At the end of the time evolution, non-zero value of KE_s is mainly due to the presence of swirls, i.e. due to the vortices, and sound propagation; Fig. 3(b) shows the change in KE_s with time. In case

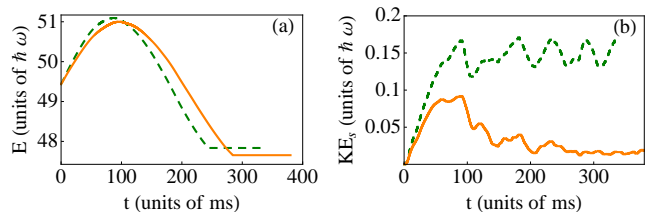


FIG. 3: (Color online) Variation of (a) E and (b) KE_s with time. The dashed dark green curve shows the variation when the obstacle is moving with the speed of $175 \mu\text{m/s}$. The solid orange curve shows the variation when the obstacle is moving with the speed of $150 \mu\text{m/s}$.

when the obstacle moves with the speed of $175 \mu\text{m/s}$, the $KE_s \sim 0.15\hbar\omega$ can be mainly ascribed to the swirls. On the other hand, when the obstacle moves with the speed of $150 \mu\text{m/s}$, swirls are only present at boundary of the SFG due to the creation of ghost vortices (vortices in low density regions). These ghost vortices do not contribute to KE_s . Hence the non-zero value of KE_s can be mainly ascribed to remnant sound waves in the superfluid. Although somewhat indistinct, the density ripples created by the sound are present in the central region of Fig. 1(c).

In the oblate condensates, the small length of vortex lines along axial direction (see Fig. 4) makes them less susceptible to vortex bending and hence vortex reconnections. This is due the suppression of Kelvin generation in oblate superfluids [48]. As a result, the vortex dipoles formed in pan-cake shaped traps are quite stable against reconnections and vortex antivortex annihilation. This is demonstrated in Fig. 4, here the superfluid density, phase, and isodensity surface with isovalue of $0.002a_{\text{osc}}^{-3}$ are shown after 334 ms of evolution.

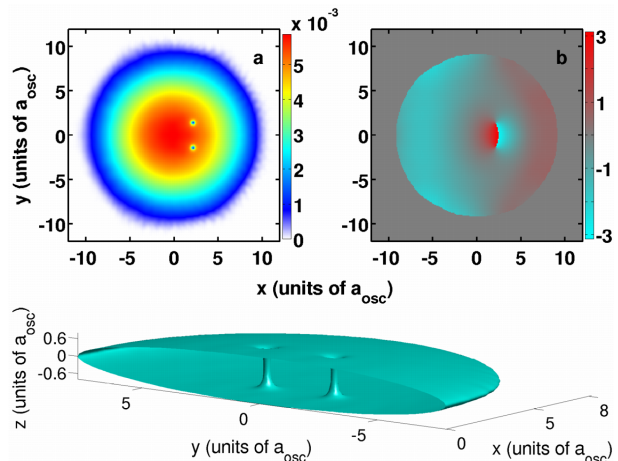


FIG. 4: (Color online) In upper row, images with labels (a) and (b) show the density and phase of the Fermi superfluid at 334 ms. In lower row, half of the isosurface of the superfluid at 334 ms clearly shows the presence of two straight vortex lines. The isosurface corresponds to $|\phi(\mathbf{r})|^2 = 0.002a_{\text{osc}}^{-3}$.

We wish to emphasize that the NLSE can not account for the presence of normal fluid in the system, and hence leads to the zero densities at the centers of the vortices.

Although very small at $T = 0$ K, the normal fluid, which predominantly occupies the vortex cores, significantly reduces the density depletion inside the vortex cores [49–55].

III. SHOCK WAVES AND SNAKE INSTABILITY IN BCS SUPERFLUIDS

As mentioned in the Sec. I, soliton mediated decay of shock waves in sufficiently wide traps can also lead to the formation of vortex dipoles. To numerically study it, we create shock waves in the BCS superfluid Fermi gas by non-adiabatically merging the two superfluid fragments. The superfluid fragments are obtained by using the Gaussian obstacle potential along y -axis and z -axis, i.e.,

$$V_{\text{obs}}(\mathbf{r}, t) = V_0 \exp \left\{ -2 \frac{[x - x_0(t)]^2}{w_0^2} \right\}. \quad (7)$$

We consider $V_0 = 93 \hbar \omega$, $x_0(t) = 0$, and $w_0 = 2.5 \mu\text{m}$ as the amplitude and width of the obstacle potential. The stationary solution with this obstacle potential is shown in Fig. 5(a). We achieve the non-adiabatic merging of the

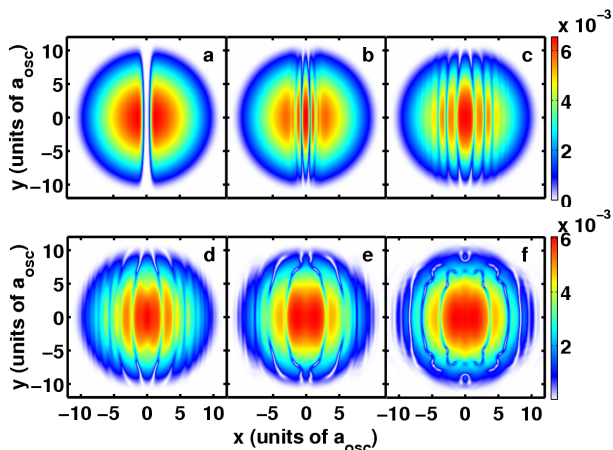


FIG. 5: (Color online) Evolution of the superfluid density $|\phi(\mathbf{r}, t)|^2$ in units of a_{osc}^{-3} after the sudden merging of the two superfluid fragments. Images with labels (a), (b), (c), (d), (e), and (f) are the densities at $t = 0$ ms, 4.8 ms, 12.7 ms, 20.7 ms, 28.6 ms, and 36.6 ms respectively.

two fragments of the superfluid by switching off the obstacle potential suddenly, and then letting the superfluid to evolve. After the obstacle potential is switched off at $t = 0$ ms, there is the formation central peak as is shown in Fig. 5(b) at 4.8ms. This is consistent with the formation of central peak after the collision of two strongly interacting Fermi gas clouds in cigar-shaped trap [8]. The central peak is bounded by two band solitons which move outward as is shown in Fig. 5(c-d). The formation of the regions with large density gradients (see Fig. 5(b-c)) can be inferred as one of the signatures of the formation of shock wave. The development of large density gradients in superfluid, during the propagation of the shock wave,

is also accompanied by large gradients in velocity field. Now, multiplying Eq. 2 by ψ^* and subtracting the resultant equation from its complex conjugate, one gets

$$\frac{\partial |\psi|^2}{\partial t} + \nabla \cdot \left[\frac{\hbar}{4mi} (\psi^* \nabla \psi - \psi \nabla \psi^*) \right] = 0$$

Comparing it with the continuity equation for the superfluid density $|\psi(\mathbf{r}, t)|^2$, the velocity field of the superfluid is

$$\mathbf{v} = \frac{\hbar}{4mi} \frac{(\psi^* \nabla \psi - \psi \nabla \psi^*)}{|\psi|^2}. \quad (8)$$

Using this equation, the velocity field of the superfluid during the initial stages of the evolution is shown in Fig. 6, clearly showing the development of large velocity gradients. As is evident from Fig. 6, there are larger gradi-

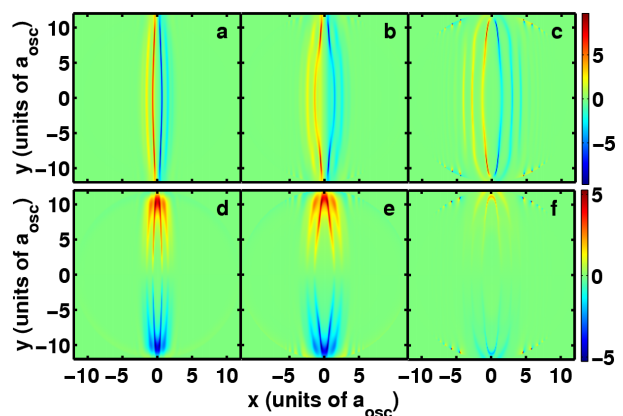


FIG. 6: (Color online) The upper and lower row show the x and y components of the velocity field respectively, in scaled units ($a_{\text{osc}}\omega$). Images with labels (a), (b) and (c) are the x component of the velocity field at $t = 4.8$ ms, 8 ms, and 12.7 ms respectively; exactly below them are the corresponding y component of the velocity field.

ents in x component of the velocity field as compared to y component, indicative of the fact the potential barrier was along y axis.

After some time, the soliton pair bounding the central peak starts to undergo snake instability [see Fig. 5(d-e)] leading to formation of the vortex dipoles [see Fig. 5(f) and 7(a)]. By this time, the outer soliton pair also starts showing signatures of snake instability [see Fig. 5(f)]. This soliton pair also decays into vortex antivortex pairs, Fig. 7(a-c). The three dimensional character of the vortex dipoles thus generated is evident from isodensity image in the lower panel of Fig. 7.

IV. CONCLUSIONS

We have studied the generation of vortex dipoles in weakly interacting pancake-shaped Fermi superfluid at $T = 0$ K using a NLSE. We find that the supercritical motion of the repulsive obstacle across the BCS superfluid leads to the generation of vortex dipoles, whereas the

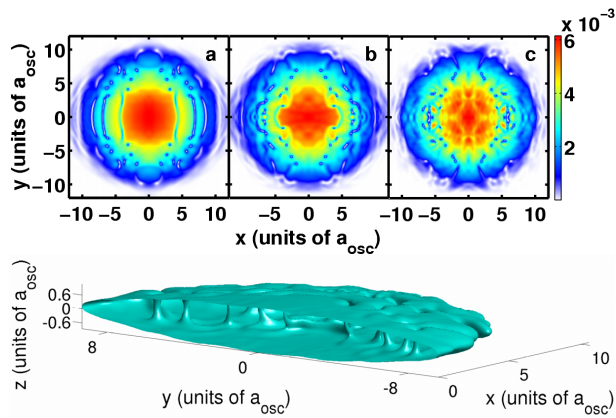


FIG. 7: (Color online) Images with labels (a), (b), (c), are the superfluid densities at $t = 44.6$ ms, 52.5 ms, and 60.5 ms respectively. In the lower panel, half of the isosurface of the superfluid at $t = 52.5$ ms clearly shows the presence of five vortex dipoles. The isosurface corresponds to $|\phi(\mathbf{r})|^2 = 0.001 a_{\text{osc}}^{-3}$.

sub-critical motion can generate only sound waves. We also observe the decay of shock waves, which are generated by sudden merging of the superfluid fragments into vortex dipoles. The strong trapping force along axial direction provides stability to vortex dipoles against vortex reconnections and vortex-antivortex annihilation events. This is responsible for the formation the dipoles which can persist for several seconds in the superfluid.

Acknowledgments

We thank Arko Roy, S. Chattopadhyay, Vivek Vyas and Dilip Angom for very useful discussions. The numerical computations reported in the paper were done on the 3 TFLOPs cluster at PRL.

-
- [1] M. Zwierlein, J. Abo-Shaeer, A. Schirotzek, C. Schunck, and W. Ketterle, *Nature* **435**, 1047 (2005).
- [2] T. W. Neely, E. C. Samson, A. S. Bradley, M. J. Davis, and B. P. Anderson, *Phys. Rev. Lett.* **104**, 160401 (2010).
- [3] B. Anderson, P. Haljan, C. Regal, D. Feder, L. Collins, C. Clark, and E. Cornell, *Phys. Rev. Lett.* **86**, 2926 (2001).
- [4] D. R. Scherer, C. N. Weiler, T. W. Neely, and B. P. Anderson, *Phys. Rev. Lett.* **98**, 110402 (2007).
- [5] Z. Dutton, M. Budde, C. Slowe, and L. Hau, *Science* **293**, 663 (2001).
- [6] W. Wan, S. Jia, and J. Fleischer, *Nature Physics* **3**, 46 (2006).
- [7] J. J. Chang, P. Engels, and M. A. Hofer, *Phys. Rev. Lett.* **101**, 170404 (2008).
- [8] J. Joseph, J. Thomas, M. Kulkarni, and A. Abanov, *Phys. Rev. Lett.* **106**, 150401 (2011).
- [9] A. Bulgac, Y.-L. Luo, and K. J. Roche, *Phys. Rev. Lett.* **108**, 150401 (2012).
- [10] L. Salasnich, *EPL (Europhysics Letters)* **96**, 40007 (2011).
- [11] C. Barenghi, R. Donnelly, and W. Vinen, *Quantized vortex dynamics and superfluid turbulence*, vol. 571 (Springer Verlag, 2001).
- [12] V. L. Berezinskii, *Soviet Journal of Experimental and Theoretical Physics* **32**, 493 (1971).
- [13] J. M. Kosterlitz and D. J. Thouless, *J. Phys. C: Solid State Physics* **6**, 1181 (1973).
- [14] A. Bulgac, Y. Luo, P. Magierski, K. Roche, and Y. Yu, *Science* **332**, 1288 (2011).
- [15] J. Chin, D. Miller, Y. Liu, C. Stan, W. Setiawan, C. Sanner, K. Xu, and W. Ketterle, *Nature* **443**, 961 (2006).
- [16] J. Hubbard, *Proceedings of the Royal Society of London. Series A. Mathematical and Physical Sciences* **276**, 238 (1963).
- [17] U. Schneider, L. Hackermüller, S. Will, T. Best, I. Bloch, T. A. Costi, R. W. Helmes, D. Rasch, and A. Rosch, *Science* **322**, 1520 (2008).
- [18] R. Jördens, N. Strohmaier, K. Günter, H. Moritz, and T. Esslinger, *Nature* **455**, 204 (2008).
- [19] A. Georges, G. Kotliar, W. Krauth, and M. J. Rozenberg, *Rev. Mod. Phys.* **68**, 13 (1996).
- [20] W. Metzner and D. Vollhardt, *Phys. Rev. Lett.* **62**, 324 (1989).
- [21] R. W. Helmes, T. A. Costi, and A. Rosch, *Phys. Rev. Lett.* **100**, 056403 (2008).
- [22] Y.-H. Chen, W. Wu, H.-S. Tao, and W.-M. Liu, *Phys. Rev. A* **82**, 043625 (2010).
- [23] W. Wu, Y.-H. Chen, H.-S. Tao, N.-H. Tong, and W.-M. Liu, *Phys. Rev. B* **82**, 245102 (2010).
- [24] Y.-H. Chen, H.-S. Tao, D.-X. Yao, and W.-M. Liu, *Phys. Rev. Lett.* **108**, 246402 (2012).
- [25] P. Wang, Z.-Q. Yu, Z. Fu, J. Miao, L. Huang, S. Chai, H. Zhai, and J. Zhang, *Phys. Rev. Lett.* **109**, 095301 (2012).
- [26] L. W. Cheuk, A. T. Sommer, Z. Hadzibabic, T. Yefsah, W. S. Bakr, and M. W. Zwierlein, *Phys. Rev. Lett.* **109**, 095302 (2012).
- [27] H. Zhai, *International Journal of Modern Physics B* **26**, 1230001 (2012).
- [28] R. Liao, Y. Yi-Xiang, and W.-M. Liu, *Phys. Rev. Lett.* **108**, 080406 (2012).
- [29] L. Salasnich, *Laser physics* **19**, 642 (2009).
- [30] Y. E. Kim and A. L. Zubarev, *Physics Letters A* **327**, 397 (2004), ISSN 0375-9601.
- [31] Y. E. Kim and A. L. Zubarev, *Phys. Rev. A* **70**, 033612 (2004).
- [32] N. Manini and L. Salasnich, *Phys. Rev. A* **71**, 033625 (2005).
- [33] G. Diana, N. Manini, and L. Salasnich, *Phys. Rev. A* **73**, 065601 (2006).
- [34] L. Salasnich and N. Manini, *Laser Physics* **17**, 169 (2007).
- [35] S. Adhikari and B. Malomed, *EPL (Europhysics Letters)* **79**, 50003 (2007).
- [36] S. K. Adhikari and B. A. Malomed, *Phys. Rev. A* **76**, 043626 (2007).
- [37] L. Salasnich, N. Manini, and F. Toigo, *Phys. Rev. A* **77**, 043609 (2008).

- [38] S. Adhikari, The European Physical Journal D-Atomic, Molecular, Optical and Plasma Physics **47**, 413 (2008).
- [39] L. Landau and E. Lifshitz, *Statistical Physics, Part 2: Theory of the Condensed State, Course of Theoretical Physics*, vol. 9 (Pergamon Press, London, 1987).
- [40] A. Leggett, *Quantum Liquids* (Oxford Univ. Press, Oxford, 2006).
- [41] S. Giorgini, L. Pitaevskii, and S. Stringari, Rev. Mod. Phys. **80**, 1215 (2008).
- [42] L. Salasnich, N. Manini, and A. Parola, Phys. Rev. A **72**, 023621 (2005).
- [43] L. Salasnich, Phys. Rev. A **76**, 015601 (2007).
- [44] C. Buitrago and S. Adhikari, J Phys. B: At. Mol. Opt. Phys. **42**, 215306 (2009).
- [45] P. Muruganandam and S. Adhikari, Computer Physics Communications **180**, 1888 (2009).
- [46] H. Heiselberg, Phys. Rev. A **73**, 013607 (2006).
- [47] P. Capuzzi, P. Vignolo, F. Federici, and M. P. Tosi, Phys. Rev. A **73**, 021603 (2006).
- [48] S. J. Rooney, P. B. Blakie, B. P. Anderson, and A. S. Bradley, Phys. Rev. A **84**, 023637 (2011).
- [49] G. M. Bruun and L. Viverit, Phys. Rev. A **64**, 063606 (2001).
- [50] M. Rodriguez, G.-S. Paraoanu, and P. Törmä, Phys. Rev. Lett. **87**, 100402 (2001).
- [51] N. Nygaard, G. M. Bruun, C. W. Clark, and D. L. Feder, Phys. Rev. Lett. **90**, 210402 (2003).
- [52] A. Bulgac and Y. Yu, Phys. Rev. Lett. **91**, 190404 (2003).
- [53] N. Nygaard, G. M. Bruun, B. I. Schneider, C. W. Clark, and D. L. Feder, Phys. Rev. A **69**, 053622 (2004).
- [54] J. Tempere, M. Wouters, and J. T. Devreese, Phys. Rev. A **71**, 033631 (2005).
- [55] R. Sensarma, M. Randeria, and T.-L. Ho, Phys. Rev. Lett. **96**, 090403 (2006).